


Molecular Dynamic Study of *B. subtilis* Laccase Against POME Waste Components with Temperature Variations and Adjustment of Active Site Mutations

Hafizh Zahra ^{1,*} , Laksmi Ambarsari ¹, Inda Setyawati ¹, Gusnia Meilin Gholam ¹, Setyanto Tri Wahyudi ^{2,*}

¹ Department of Biochemistry, Faculty of Mathematics and Natural Sciences, IPB University, Bogor, 16680, Indonesia; hafizhahra@apps.ipb.ac.id (H.Z.); laksmi@apps.ipb.ac.id (L.A.); inda_setyawati@apps.ipb.ac.id (I.S.); gusnia_26@apps.ipb.ac.id (G.M.G.);

² Department of Physics, Faculty of Mathematics and Natural Sciences, IPB University, Bogor, 16680, Indonesia; stwahyudi@apps.ipb.ac.id (S.T.W.);

* Correspondence: stwahyudi@apps.ipb.ac.id (S.T.W.); hafizhahra@apps.ipb.ac.id (H.Z.);

Scopus Author ID 57191576360

Received: 8.10.2022; Accepted: 15.11.2022; Published: 31.01.2023

Abstract: One type of liquid waste produced by Crude Palm Oil processing is Palm Oil Mill Effluent (POME). This waste is a big challenge for the environment because of its dark brown color and rich in organic compounds. Its brownish color comes from melanoidin, a pigment produced by the Maillard reaction of processed coconut, whereas its organic compounds come from several components. The predominantly common bacteria in POME bioremediation is *Bacillus subtilis* species, notably because of its thermostable laccase. Various researchers performed several mutations to enhance its dye-degrading capability. However, most result either in increased K_M or unstable. This study aimed to produce recommendations for stabilizing mutant construction, followed by molecular docking and molecular dynamics (MD) of POME components. We performed mutant construction and structure evaluation using the PoPMuSiC-2.1 server while ligand-receptor preparation, molecular docking, and MD by YASARA Structure. After minimization, the results showed the energy difference from the optimized T480V mutant from 73.98 to -95.04 kcal/mol. Caffeic acid has the highest docking score, whereas the different temperature of MD reveals that increased temperature (80 °C) improve melanoidin binding energy. Nevertheless, the need for further studies will strengthen previously existing results.

Keywords: POME bioremediation; *Bacillus subtilis*; temperature; mutation; molecular docking; molecular dynamics.

© 2023 by the authors. This article is an open-access article distributed under the terms and conditions of the Creative Commons Attribution (CC BY) license (<https://creativecommons.org/licenses/by/4.0/>).

1. Introduction

Every process of processing oil palm fresh fruit bunches into crude palm oil will generate solid and liquid waste. Palm Oil Mill Effluent (POME) is one form of liquid waste. It is estimated that palm oil processing mills can produce 455,000 tons of POME waste per day in Indonesia [1]. POME will harm the aquatic environment without proper treatment by blocking surface light [2]. It is suspected that the color of POME waste comes from melanoidin, a toxic biopolymer pigment produced by the Maillard reaction of coconut processing. In addition, there are other phytotoxic components such as o-cresol, m-cresol, 4-hydroxybenzoic acid, 3-methylcatechol, caffeic acid, and ferulic acid [3,4]. Based on this, oxidoreductase-type

enzymes have strong biodegradation capabilities of dyes and phenolic components as an alternative to green solutions.

One of the most widely used enzymes in the bioremediation of POME waste is laccase from *Bacillus subtilis* species in axenic or consortium cultures. Research by Sharma and Mittal [5] showed that the axenic culture of *B. subtilis* could degrade melanoidin by 62.5% [6]. *B. subtilis* laccases were also categorized as thermostable compared to other sources. One mutation (T480A) was found to increase laccase activity by 2.38 times, despite having a significant increase in KM due to the low alanine β -sheet propensity [7,8]. Based on this, rational protein design is needed for stable mutant construction.

Furthermore, it is possible to increase the catalytic efficiency of the *B. subtilis* laccase enzyme through point mutations because it has been crystallized and deposited in the Protein Data Bank [8]. This result is also supported by the new active site (extrusion loop) of *B. subtilis* laccase by Liu *et al.* [8], which was co-crystallized with ABTS (2,2-azinobis-3-ethylbenzothiazoline-6-sulfonate), a free radical. The extrusion loop (residue 359-365) and the region around domain 3 of the *B. subtilis* laccase enzyme have not been studied further regarding their catalytic efficiency apart from the ABTS ligand. Therefore, studies on mutagenesis and MD simulation with POME waste components can broaden the view of its bioremediation potential.

This study aims to produce recommendations for mutant construction based on *in vitro* studies by Bu *et al.* [9] with the help of a web server. Further molecular docking was carried out between the mutant and wild-type structures with the phenolic component of POME waste to obtain a ligand-receptor complex. The mutant form was then treated with temperature variations in MD simulations and compared with the wild type based on several dynamics parameters.

2. Materials and Methods

The tools used in the research are Dell Inspiron 15 7000 type laptop with Intel® Core™ i7-7700HQ processor equipped with 16 GB RAM and Windows 10 as the primary operating system. The software used is YASARA (Yet Another Scientific Artificial Reality Application) with the FoldX4 plugin, MarvinView 6.0.0, and Discovery Studio 3.5 Client. Supporting servers include PubChem (<https://pubchem.ncbi.nlm.nih.gov/>) and PoPMuSiC version 2.1 (<https://soft.dezyme.com/>).

The primary material used in this study was the crystal structure of the laccase CotA *B. subtilis* (PDB ID: 4YVN) with a resolution of 2.3 Å. The ligands used in the *in silico* test were the chemical structures of o-cresol, m-cresol, 4-hydroxybenzoic acid, 3-methylcatechol, caffeic acid, and ferulic acid compounds obtained from PubChem. Melanoidin structures were created manually using Chem3D.

2.1. Mutant construction and structure evaluation.

The PoPMuSiC-2.1 server calculated the folding free energy through model analysis. PoPMuSiC-2.1 is an online program that predicts the fold-free energy changes regarding the thermodynamic stability of proteins resulting from single-site mutations. The expected change in folding free energy ($\Delta\Delta G$) was expressed using a linear combination of the statistical potential with solvent accessibility-dependent coefficients of the mutated residue [48]. After obtaining the potential residues in domain 3 of the laccase structure, the mutation process can

be carried out. The mutation of concern to the wild form is the T480 adjustment from the research of Jia *et al.* [7]. Mutations were carried out in YASARA software using the FoldX 4 plugin for the 32-bit Windows version (<http://foldx.crg.es>). The FoldX executable file is selected in the configure plugin sub-menu in the analyze menu before choosing the rotabase file [10]. As for laccase, a mediator with high redox potential is needed for result comparison with other ligand results. "Mediators" are a class of low-molecular-weight compounds with high redox potential (above 900 mV) and could increase the catalytic activity of laccases. According to Song *et al.* [49], the well-known mediators, ABTS (2,2'-azino-bis(3-ethylbenzothiazoline-6-sulfonic acid), can run numerous cycles without degrading or causing any side effects. It diffuses outside the enzymatic pocket after the enzyme has oxidized, producing a highly oxidizing intermediate called an oxidized mediator.

2.2. Receptor and ligand preparation.

Preparation of all ligands and receptors was carried out using YASARA Structure. The three-dimensional (3D) structures of the comparison ABTS and test ligands were downloaded via PubChem in (.sdf) format. All ligands are added with hydrogen atoms, and energy minimization is carried out. The energy minimization process will produce the minimum inter-atomic energy values and form a more stable and optimal molecular conformation before being stored in pdb format [11–14]. After all the ligands were prepared, we combined the test and comparison ligands to save in the YASARA file (_ligands.sdf) for molecular docking [15–17].

Receptor preparation is done by trimming the structure from water and unwanted ligands. Then the receptor was further optimized by adding polar hydrogen and the AMBER14 (Assisted Model Building with Energy Refinement) force field [12,18,19]. The conformity of the enantiomers, the absence of cis-peptide bonds, the normality of the length and bond angles, and the dihedral angle of the structure were then checked using the menu 'Analyze' on YASARA.

2.3. Molecular docking validation and simulation.

The validation process is carried out by targeted docking. The ligand docking zone is bounded by a cuboid gridbox around the active site of the extruding loop. Gridbox validation was initiated by redocking the comparison ligand 999 times (macro dock_runlocal) [18,20]. The gridbox size ranges from 0-5 to get the best binding affinity and root-mean-square deviation (RMSD) values [20]. The results with the best gridbox sizes were visualized using the Discovery Studio 2021 Client [21]. The molecular docking simulation used the YASARA structure [22,23] by docking all test ligands to wild-type and mutant-type receptors, where the ligand shape was fixed. The command file is dock_runscreening with 999 repetitions and determining the best pose. The program in the macro file is AutoDock4, using the LGA (Lamarckian Genetic Algorithm) method [15,20,24–26].

2.4. Molecular dynamics simulation, modification from Mahtarin et al. [27].

The AMBER14 force field is used for the calculation of the MD parameter. Berendsen thermostats and Particle Mesh Ewald were selected to regulate the system temperature and pressure during the simulation. The equilibrated system environment was equilibrated with 0.9% NaCl (pH 4.0), and water solvent (0.997 g/mL) at a temperature of 310 K. After the environment was equilibrated, the simulation was carried out again with temperature

variations. Martins *et al.* [28] research explained that the highest activity was obtained at a temperature of 75 °C. Based on Cho *et al.* [28], *B. subtilis* laccase also showed the highest activity at 80 °C. Thus, the simulation temperature variations will occur at 30 °C and 80 °C. The water density selected was 0.99571 g/mL (30 °C) and 0.97176 g/mL (80 °C) with Manometer1D and 3D activation. The receptor manometer, before docking, also performed an MD simulation with the same parameters.

The complex resulting from the molecular docking of previous studies with the best free energy values was selected and stored as a YASARA scene (.sce). The simulation is done by selecting the target and then running it based on the md_run macro command. The simulation is carried out for 50 ns (50000 ps) with a snapshot every 5000000 fs. After MD simulation, Root Mean Square Deviation (RMSD), Root Mean Square Fluctuation (RMSF), Solvent Accessible Surface Area (SASA), the radius of gyration, the total number of hydrogen bonds, and two-dimensional structure data were collected for further analysis.

2.5. Analysis of simulation results and calculation of binding energy, modification from Maulana [29].

Trajectories in sim and HTML formats obtained from the simulation were analyzed using YASARA. The MD analysis performed included RMSD, RMSF, non-bonding energy, solvent accessibility (SASA), secondary structure changes, salt bridges, hydrogen bonds, and structural visualization of both holo and apo forms. In addition, the hydrogen bond formed is calculated at a distance between the donor and acceptor atoms of 3, while for the salt bridge, the cutoff distance value of oxygen and nitrogen atoms is 3.2. Each snapshot of the analysis results in the form of "sim" is converted to pdb. The conformational changes are then visualized using Discovery Studio Client 3.5 in 2D and 3D (surface dan solid ribbon).

3. Results and Discussion

3.1. Mutant construction.

We used PopMuSiC to help predict the change in fold-free energy upon mutation ($\Delta\Delta G$). A negative value in the ΔG score indicates a mutation that is predicted to be stabilizing. Mutations are changes in genetic sequences and are known to be the leading cause of diversity among organisms, and these changes can occur at many different levels with various consequences [30]. There are two concerns in capturing mutations in active site positions around the extrusion loop. First is the magnitude of the decrease in $\Delta\Delta G$ (folding mutation), representing the folding free energy shift due to a mutation. The second is amino acid propensity congruence by comparison with another amino acid. Propensity signifies a relative quantity of the amino acid frequency occurring in a secondary structure in a specific fold [50]. The secondary structure should not be mismatched (e.g., between α -helix and β -sheets) to provide a valid rational protein design.

This study shows that wild-type structure (WT) Threonine position 480 preferred strand conformation with a propensity score of 1.17, while valine by 1.87. Additionally, the PopMuSiC server result demonstrates the decrease in $\Delta\Delta G$ by 0.01 kcal/mol from threonine to valine (supplementary 1). This results indicate that valine had a greater strand propensity due to its branching side chain than threonine (Figure 1). After selecting valine as the amino acid of the mutation, the mutation's result was T480V. The T480V mutant was further minimized using FoldX to repair bad torsion angles, Van der Waals clashes, and total energy.

The initial energy of the T480V mutant is 73.98 kcal/mol. After energy minimization, it decreased to -95.04 kcal/mol.

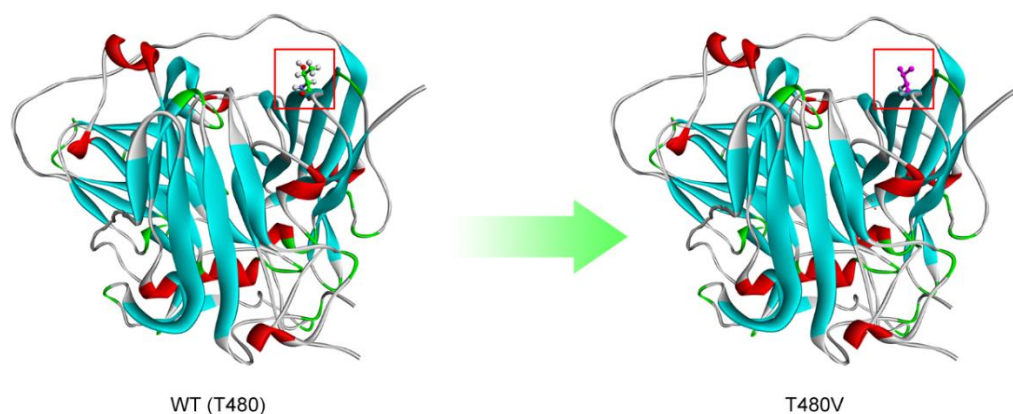


Figure 1. Mutant construction.

3.2. Molecular docking.

Before molecular docking, we validated gridbox via ABTS redocking, a comparative yet staple ligand for multicopper oxidases. Docking targets are extruding active loop sites (359-365). Gridbox is selected based on the highest energy binding and looking at RMSD. Beneath extruding loop contain the positively charged area, mainly comprised of Arginine residue (429 and 476), and is thought to be essential for phenolic components oxidation [7,8,31,32].

Based on Table 1, the Gridbox with a size of 20.96 Å was chosen because it has a binding energy of -9.06 kcal/mol, a dissociation constant of 0.23 µM, and an RMSD of 0.4675 Å. Ideally, the RMSD used in the computational method is said to be valid and well-bound when the RMSD value is less than 2.0 Å [33].

Table 1. Gridbox Validation.

Gridbox (Å)	Binding energy (kcal/mol)	Dissoc. Constant (µM)	RMSD (Å)
14.96	-9.00	0.25	0.3787
15.96	-9.06	0.23	0.4785
16.96	-9.06	0.23	0.4644
17.96	-9.05	0.23	0.4608
18.96	-9.06	0.23	0.4664
19.96	-9.05	0.23	0.4826
20.96	-9.06	0.23	0.4675

Based on the gridbox validation visualization analysis results, ABTS forms interactions with receptors in the form of van der Waals, hydrogen bonds, salt bridges, conventional hydrogen bonds, carbon-hydrogen bonds, Pi-Sigma, Pi-Sulfur, Pi-Pi Stacked, Pi-Pi T-shaped, and Pi-Alkyl (Figure 2). These types of bonds and interactions, which we suggest and may become the primary reference in this study and other studies. The Lamarckian Genetic Algorithm (LGA) was implemented to filter and select the best docking poses. The interaction energy provides insight into the strength of the forces between protein-ligand interactions [22,23,25]. The results of the docking can be seen in Table 2.

Table 2. T480V mutant molecular docking results.

Ligand	PubChem CID	Binding energy (kcal/mol)	Dissoc. Constant (µM)
ABTS	9570474	-8.82	0.34
Caffeic acid	689043	-5.41	107.79
Ferulic acid	445858	-5.23	147.49

Ligand	PubChem CID	Binding energy (kcal/mol)	Dissoc. Constant (μM)
4-hydroxybenzoic acid	135	-4.63	401.28
m-cresol	342	-3.97	1230
3-methylcatechol	340	-3.92	1340
o-cresol	335	-3.79	1670
Melanoidin	-	-3.19	4590

T480V mutant paired best with caffeic acid from all ligands by binding energy -5.41 kcal/mol and dissociation constant 107.79 μM . In addition, docking results in a binding energy range of -3.19 to -8.82 kcal/mol. Binding energy is a critical stability manifestation between the ligand and the receptor [33,34]. According to the structure deposited by Liu et al. [8], the active site surrounding extruding loop is found in the residues Ser360, His363, Trp43, Thr480, and Ala479. Whereas area representing substrate binding site are Thr406, Ile408, Leu431, Trp463, Arg476, Ala478, Ala479, and Thr480 (Valine substitution). Furthermore, Arg429 and Ser427 are essential amino acid residues for oxidizing phenolic compounds and dye molecules. These residues are known for providing catalytic properties and are highly conserved among fungal and bacterial laccases. This experiment only focused on the extruding loop, a novel substrate-binding site for the oxidation of numerous substrates, not laccase's copper center (which contains catalytic activity on reducing oxygen to water). As additional information, the distance between the copper center to the Val480 position is 17.96 Å.

The complex of caffeic acid with T480V (Figure 3) forms hydrogen bonds with the residues Ser360, Ser427, Ala479, and Phe428. The hydrogen bond formed caused by the hydroxyl group (OH) on the caffeic acid ligand has amino acid residue contacts with Ser360 and Ser 427, while Ala479 and Phe428 have oxygen atomic contact. The Pi-Anion bond in this complex, Glu364, connects with the aromatic ring on the caffeic acid ligand. Ferreira de Freitas and Schapira [35] explained that electrostatic bonding could determine the maximum efficiency of ligand binding.

Melanoidin complexes with mutant T480V (Figure 3) also form Van der Waals and hydrogen bonds. Hydrogen bonds are created because the ligand's hydroxyl group (OH) has contact with Glu364, Ser427, and Ala478, while Val480 has hydrogen bonds with the oxygen atom in the ligand and Ala478 has contact with the hydrogen atom in the ligand. In addition, hydrogen bonding is caused by the amine on the ligand with the Glu364 amino acid residue on the receptor. We found a Pi-Sigma bond in this complex, the ligand hydrogen atom having contact with the His363 amino acid residue. Melanoidin shows considerable binding affinity as a bulky ligand at -3.19 kcal/mol. The active site is also found in the amino acid residues Val480, Ala478, Phe428, His363, and Ser360.

Hydrogen bonding is a directed intermolecular interaction in biological complexes and contributes significantly to the specificity of molecular recognition [35]. *In silico* studies suggest that the greater the interaction of hydrogen bond interactions between enzymes and ligands, the greater the binding strength [36]. Other studies have explained that hydrogen and electrostatic bonds are essential in stabilizing the complex [37]. Each complex formed in this study comprises a Van der Waals interaction. The existence of Van der Waals interactions can occur in charged residues and uncharged residues. This interaction occurs due to a relatively weak electrical attraction due to permanent or induced molecular polarity [38].

Hydrogen bonds often appear in organic compounds, such as peptides and polymers. In addition, this type of bond can cause rotation of the main chain of the peptide or polymer [39]. The stronger the intermolecular hydrogen bonds, the easier it is predicted that the transfer of protons between molecules will be more accessible [40].

Intermolecular interaction is a fundamental concept known for a long time. The idea aims to explain the phenomena and macroscopic properties that appear in the field of chemistry. Various intermolecular interactions such as dipole-dipole bonds, dipole-ions, induced dipole-dipole, Van der Waals bonds, hydrogen bonds, London forces, and hydrophobic and hydrophilic effects play a role in binding efficiency [39].

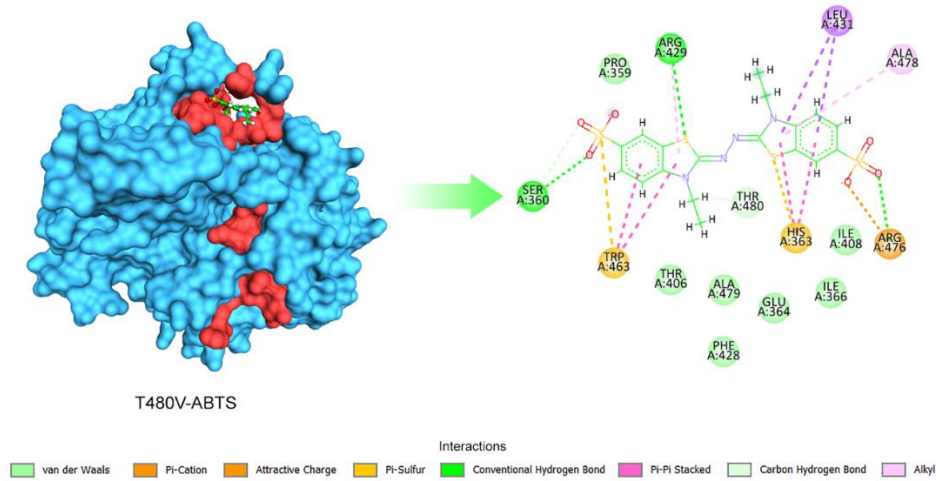


Figure 2. Visualization of ABTS validation results (20.96 Å gridbox).

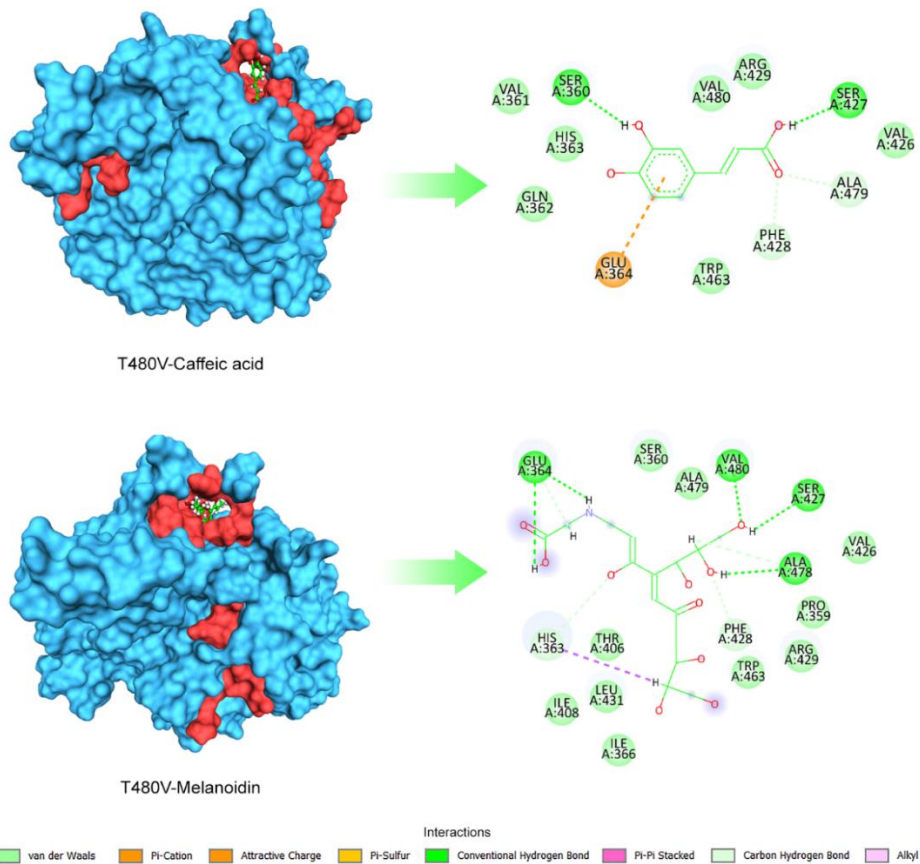


Figure 3. Visualization of the docking complex results (caffeic acid and melanoidin).

3.3. Molecular dynamics simulation.

Molecular dynamics (MD) simulation has edges over molecular docking. MD can support predictions in the binding mode and can also indicate conformational shifts in protein-

ligand complexes [41–44]. First, we did MD on ABTS with T480V mutant with two temperature variations, 30 °C, and 80 °C, with a simulation time of 50 ns. Based on Cho et al. [28], laccase-expressing *B. subtilis* spores showed their highest activity level for oxidizing ABTS with 100% relative activity at pH 4.0 and 80 °C. The initial temperature used in the initial temperature treatment is 30 °C, so the temperature range is as follows. The temperature variation in this study affects the binding energy significantly (Table 3). The estimated decrease in ABTS binding energy from 80 °C to 30 °C is around 14 kcal/mol. This result indicates ABTS interacts best in higher temperatures, identical to the earlier studies [45,46].

Through 250 data, melanoidin binding energy increased by 47 kcal/mol from 30 °C to 80 °C. The positive value of binding energy might indicate several "unbinding" phases of melanoidin. However, some spiking at 80 °C increased binding energy hinders the positive binding energy value [45,46]. By the end of each simulation time, both started resulting in negative binding energy, possibly by favorable repositioning of the active site around the substrate. The energy released due to the bond formation, or the ligand and protein interaction, is termed binding energy. The binding energy of the favorable reaction is negative [45,46].

Table 3. The binding energy of ABTS and Melanoidin with T480V mutant.

Ligand	Simulation time (ns)	Binding energy (kcal/mol)	
		30 °C	80 °C
ABTS	5	-101.95	-35.79
	10	-64.71	-81.55
	15	-125.05	-178.93
	20	-126	-112.53
	25	-168.86	-94.15
	30	-99.75	-135.37
	35	-11.27	-72.21
	40	-207.34	-149.57
	45	-29.44	-134.77
	50	-77.96	-157.65
	Average	-101.23	-115.25
Melanoidin	5	-6.51	-4.68
	10	72.92	121.42
	15	61.35	-327.57
	20	-43.35	-232.92
	25	-24.34	13.18
	30	64.53	125.07
	35	-8.80	170.64
	40	26.16	102.05
	45	-49.93	-114.53
	50	-139.29	-245.16
	Average	-4.73	-51.93

Furthermore, the solute's molecular and solvent-permeable surface area was determined against the simulation time to help comprehend the possible binding pattern that developed during the simulation. The ABTS complex achieved equilibrium at around 16 ns (30 °C) and 6 ns (80 °C), and the complex remained reasonably stable. After this duration onwards, the backbone RMSD fluctuations (red) were found to be confined within a range of 1.4–2.6 (30 °C) and 1.5–3.2 (80 °C) (Figure 4) [46,47]. As mentioned earlier, this narrow range was considered tolerable for the plot for laccase thermostable properties. This result is linear with Jia *et al.* [7] and Liu *et al.* [8] for ABTS as a laccase's staple ligand.

For the first four ns (30 °C) and six ns (80 °C), the melanoidin complex achieved equilibrium; the complex remained reasonably stable. After this duration, the backbone RMSD fluctuations (red) were confined to 1.4–2.6 Å (Figure 4). RMSD for the laccase-melanoidin complex at a low temperature was lower than that at a higher temperature, indicating these

might be the result of enhanced stability [46,47]. However, by the end of the simulation (50 ns), the graph for both ligands fluctuated towards a higher value. Based on these results, the suggestion that researchers can give is to simulate with a longer time. This procedure might help the complex adjust its conformation with a more extended temperature adjustment.

The density fluctuates due to conformational changes in the simulated protein. Because the extra kinetic energy is partly stored as potential energy, there is a frequent significant rise in energy within the initial nanoseconds when the simulation starts from an energy-minimized "frozen" conformation. These are initially put in the lowest potential energy places, generally adjacent to charged solute groups, from which they detach to obtain entropy and potential energy [47]. The 'simulation cell' is recalibrated to maintain constant pressure during the simulation. The total potential energy of the system is plotted against the simulation time (Figure 5) [47]. For the ABTS complex, temperature increases cause the energy to drop by around 92,000 kJ/mol. While for the melanoidin complex, it can be inferred that during simulation, the system's total potential energy decreased from 30 °C to 80 °C through the end of simulation time with the same energy interval.

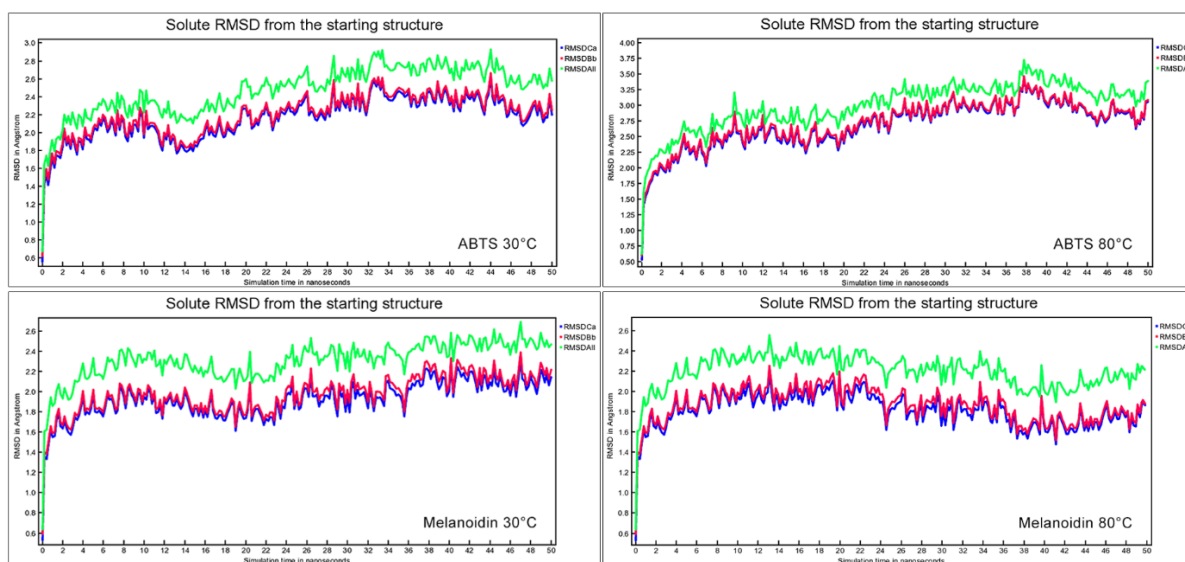


Figure 4. Solute RMSD from the starting structure plotted against the simulation time. The green line illustrates RMSD fluctuations from the all-heavy atom, the red line from the protein backbone, and the blue line from α -carbon.

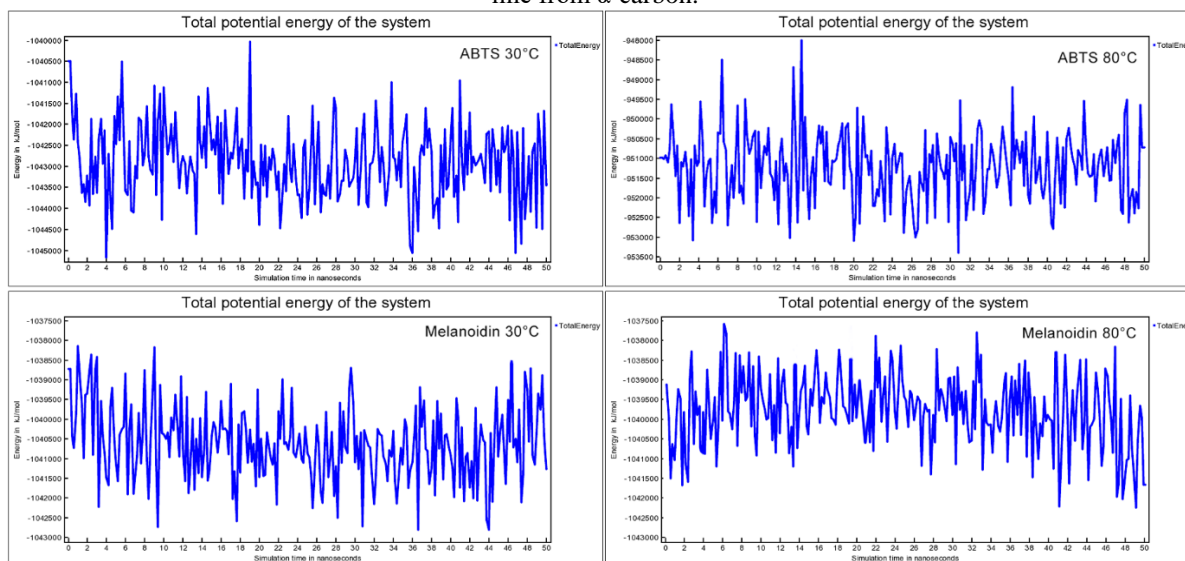


Figure 5. The total potential energy of the system is plotted against simulation time. The blue line illustrates the total potential energy fluctuation of the receptor-ligand complex according to temperature adjustments.

In the 80 °C system of the ABTS complex, both Arg429 and His363 interaction concentrated in the thiazolinone center on both sides. Proportionally stabilized ligand along with some hydrophobic bonds between Ala478 and Leu431 (Figure 6). Furthermore, for the melanoidin complex, ligand-receptor interaction formed four hydrophobic bonds within 80 °C simulations through Ile408, Ala478, Ile366, and His363. The interaction focused on the outer carbon of melanoidin, a possible nucleophile site. Notably, more receptor-active sites covered melanoidin at 80 °C (Figure 6).

Enzymes in bioremediation systems must continue functioning in acidic pH conditions or with high concentrations of organic solvents. These properties follow the biological conditions of wastewater treatment from the palm oil processing industry. Most enzymes lose their activity in this situation due to inappropriate folding [51]. Thus, laccases for industrial dye decolorization must be tolerant of organic solvents, stable over a wide pH range, and thermostable. Therefore, industrial applications of textile effluent decolorization will benefit from screening and identification of new sources of bacterial laccase with thermostable properties [52].

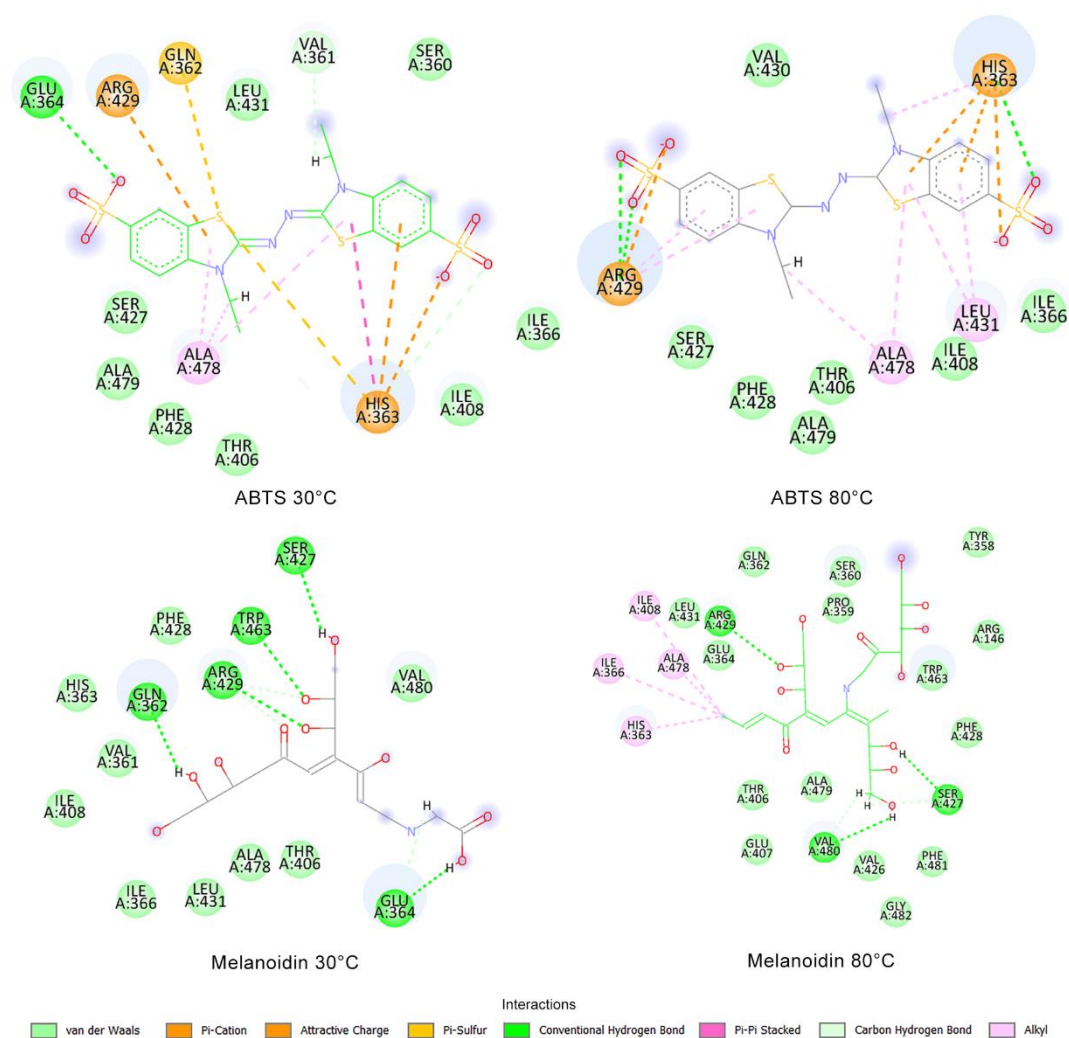


Figure 6. The molecular dynamic visualization results between ABTS and melanoidin ligand with the T480V mutant. The upper figures illustrate ABTS interaction, while the lower figures demonstrate melanoidin interaction between the two temperatures.

4. Conclusions

Based on the research results, the T480V mutant has adequate stability after energy minimization. Then the result showed that the system predicted POME waste's phenolic component to be strong enough to bind to the ligand-receptor complex via molecular docking. In the MD simulation, the temperature difference treatment for T480V shows a difference in the average binding energy. The increased temperature results in positive favorable binding energy. However, further *in vitro* studies are needed to strengthen previously existing results. Longer MD simulation duration is also needed to provide better stability for the ligand-receptor complex to adjust its conformation with a more extended temperature adjustment.

Funding

This research received no external funding.

Acknowledgments

This research has no acknowledgment.

Conflicts of Interest

The authors declare no conflict of interest.

References

1. Shintawati; Hasanudin, U.; Haryanto, A. Karakteristik pengolahan limbah cair pabrik minyak kelapa sawit dalam bioreaktor cigar semi kontinu characteristic of Palm Oil Mill Waste water treatment using semicontinue anaerobic cigar bioreactor. *Tek. Pertan. Lampung* **2017**, *6*, 81–88.
2. Ibrahim, A. H.; Dahlan, I.; Adlan, M. N.; Dasti, A. F. Comparative study on characterization of Malaysian Palm Oil Mill Effluent. *Res. J. Chem. Sci.* **2012**, *7*, 1-5.
3. Khongkhaem, P.; Suttinun, O.; Intasiri, A.; Pinyakong, O.; Luepromchai, E. Degradation of phenolic compounds in palm oil mill effluent by silica-immobilized bacteria in internal loop airlift bioreactors. *Clean - Soil, Air, Water* **2016**, *44*, 383–392, <https://doi.org/10.1002/clen.201300853>.
4. Casa, R.; D'Annibale, A.; Pieruccetti, F.; Stazi, S. R.; Sermanni, G. G.; Lo Cascio, B. Reduction of the phenolic components in olive-mill wastewater by an enzymatic treatment and its impact on durum wheat (*Triticum Durum* Desf.) Germinability. *Chemosphere* **2003**, *50*, 959–966, [https://doi.org/10.1016/S0045-6535\(02\)00707-5](https://doi.org/10.1016/S0045-6535(02)00707-5).
5. Singh, D.; Narang, E.; Chutani, P.; Kumar, A.; Sharma, K. K.; Dhar, M.; Viridi, J. S. Isolation, characterization and production of bacterial laccase from *Bacillus* sp. In *Microbial Diversity and Biotechnology in Food Security* **2014**, 439–450, https://doi.org/10.1007/978-81-322-1801-2_39.
6. Bharagava, R. N.; Chandra, R.; Rai, V. Isolation and characterization of aerobic bacteria capable of the degradation of synthetic and natural melanoidins from distillery effluent. *World J. Microbiol. Biotechnol.* **2009**, *25*, 737–744, <https://doi.org/10.1007/s11274-008-9944-7>.
7. Jia, H.; Lee, F. S.; Farinas, E. T. *Bacillus subtilis* spore display of laccase for evolution under extreme conditions of high concentrations of organic solvent. *ACS Comb. Sci.* **2014**, *16*, 665–669, <https://doi.org/10.1021/co500113t>.
8. Liu, Z.; Xie, T.; Zhong, Q.; Wang, G. Crystal structure of CotA laccase complexed with 2,2-azino-bis-(3-ethylbenzothiazoline-6-sulfonate) at a novel binding site. *Acta Crystallogr. Sect. Struct. Biol. Commun.* **2016**, *72*, 328–335, <https://doi.org/10.1107/S2053230X1600426X>.
9. Bu, T.; Yang, R.; Zhang, Y. J.; Cai, Y.; Tang, Z.; Li, C.; Wu, Q.; Chen, H. Improving decolorization of dyes by laccase from *Bacillus licheniformis* by random and site-directed mutagenesis. *PeerJ* **2020**, *8*, e10267, <https://doi.org/10.7717/peerj.10267>.
10. Chen, Y.; Luo, Q.; Zhou, W.; Xie, Z.; Cai, Y. J.; Liao, X. R.; Guan, Z. B. Improving the catalytic efficiency of *Bacillus pumilus* CotA-laccase by site-directed mutagenesis. *Appl. Microbiol. Biotechnol.* **2017**, *101*, 1935–1944, <https://doi.org/10.1007/s00253-016-7962-1>.
11. Venkatachalam, K. V.; Ettrich, R. H. Role of aspartic acid residues D87 and D89 in APS kinase domain of human 3'-phosphoadenosine 5'-phosphosulfate synthase 1 and 2b: a commonality with phosphatases/kinases. *Biochem. Biophys. Reports* **2021**, *28*, 101155,

- <https://doi.org/10.1016/j.bbrep.2021.101155>.
12. Land, H.; Humble, M. S. YASARA: A tool to obtain structural guidance in biocatalytic investigations. *Methods Mol. Biol.* **2018**, *1685*, 43–67, https://doi.org/10.1007/978-1-4939-7366-8_4.
 13. Mubarak Ali, D.; Akshaya, T.; Sathya, R.; Irfan, N. Study on the interaction of algal peptides on virulence factors of *Helicobacter pylori*: In silico approach. *Appl. Biochem. Biotechnol.* **2022**, *194*, 37–53, <https://doi.org/10.1007/s12010-021-03716-4>.
 14. Etsè, K. S.; Etsè, K. D.; Nyssen, P.; Mouithys-Mickalad, A. Assessment of anti-inflammatory-like, antioxidant activities and molecular docking of three alkynyl-substituted 3-ylidene-dihydrobenzo[d]isothiazole 1,1-dioxide derivatives. *Chem. Biol. Interact.* **2021**, *344*, <https://doi.org/10.1016/j.cbi.2021.109513>.
 15. Ur Rehman, M. F.; Akhter, S.; Batool, A. I.; Selamoglu, Z.; Sevindik, M.; Eman, R.; Mustaqeem, M.; Akram, M. S.; Kanwal, F.; Lu, C.; Aslam, M. Effectiveness of natural antioxidants against sars-cov-2? insights from the in-silico world. *Antibiotics* **2021**, *10*, 1–33, <https://doi.org/10.3390/antibiotics10081011>.
 16. Cortés-Benítez, F.; Roy, J.; Perreault, M.; Maltais, R.; Poirier, D. 16-picolyl-androsterone derivative exhibits potent 17 β -HSD3 inhibitory activity, improved metabolic stability and cytotoxic effect on various cancer cells: synthesis, homology modeling and docking studies. *J. Steroid Biochem. Mol. Biol.* **2021**, *210*, 1–13, <https://doi.org/10.1016/j.jsmb.2021.105846>.
 17. Gholam, G. M. Molecular docking of the bioactive compound ocimum sanctum as an inhibitor of sap 1 *Candida albicans*. *Sasambo J. Pharm.* **2022**, *3*, 18–24, <https://doi.org/https://doi.org/10.29303/sjp.v3i1.157>.
 18. Knape, M. J.; Wallbott, M.; Burghardt, N. C. G.; Bertinetti, D.; Hornung, J.; Schmidt, S. H.; Lorenz, R.; Herberg, F. W. Molecular basis for Ser/Thr specificity in PKA signaling. *Cells* **2020**, *9*, 1548, <https://doi.org/10.3390/cells9061548>.
 19. Gonzalez, T. L.; Rae, J. M.; Colacino, J. A.; Richardson, R. J. Homology models of mouse and rat estrogen receptor- α ligand-binding domain created by in silico mutagenesis of a human template: Molecular docking with 17 β -estradiol, diethylstilbestrol, and paraben analogs. *Comput. Toxicol.* **2019**, *10*, 1–16, <https://doi.org/10.1016/j.comtox.2018.11.003>.
 20. Patel, C. N.; Kumar, S. P.; Pandya, H. A.; Rawal, R. M. Identification of potential inhibitors of coronavirus hemagglutinin-esterase using molecular docking, molecular dynamics simulation and binding free energy calculation. *Mol. Divers.* **2021**, *25*, 421–433, <https://doi.org/10.1007/s11030-020-10135-w>.
 21. Uzzaman, M.; Hasan, M. K.; Mahmud, S.; Yousuf, A.; Islam, S.; Uddin, M. N.; Barua, A. Physicochemical, spectral, molecular docking and ADMET studies of bisphenol analogues; a computational approach. *Informatics Med. Unlocked* **2021**, *25*, 100706, <https://doi.org/10.1016/j.imu.2021.100706>.
 22. Krieger, E.; Vriend, G. YASARA view - molecular graphics for all devices - from smartphones to workstations. *Bioinformatics* **2014**, *30*, 2981–2982, <https://doi.org/10.1093/bioinformatics/btu426>.
 23. Krieger, E.; Koraimann, G.; Vriend, G. Increasing the precision of comparative models with YASARA NOVA - a self-parameterizing force field. *Proteins Struct. Funct. Genet.* **2002**, *47*, 393–402, <https://doi.org/10.1002/prot.10104>.
 24. Bilal, S.; Mudassir Hassan, M.; Fayyaz ur Rehman, M.; Nasir, M.; Jamil Sami, A.; Hayat, A. An insect acetylcholinesterase biosensor utilizing WO₃/g-C₃N₄ nanocomposite modified pencil graphite electrode for phosmet detection in stored grains. *Food Chem.* **2021**, *346*, 128894, <https://doi.org/10.1016/j.foodchem.2020.128894>.
 25. Durai, P.; Shin, H. J.; Achek, A.; Kwon, H. K.; Govindaraj, R. G.; Panneerselvam, S.; Yesudhas, D.; Choi, J.; No, K. T.; Choi, S. Toll-like receptor 2 antagonists identified through virtual screening and experimental validation. *FEBS J.* **2017**, *284*, 2264–2283, <https://doi.org/10.1111/febs.14124>.
 26. Trott, O.; Olson, A. J. AutoDock Vina: Improving the speed and accuracy of docking with a new scoring function, efficient optimization, and multithreading. *J. Comput. Chem.* **2009**, *31*, 455–461, <https://doi.org/10.1002/jcc.21334>.
 27. Mahtarin, R.; Islam, S.; Islam, M. J.; Ullah, M. O.; Ali, M. A.; Halim, M. A. Structure and dynamics of membrane protein in SARS-CoV-2. *J. Biomol. Struct. Dyn.* **2020**, *40*, 4725–4738, <https://doi.org/10.1080/07391102.2020.1861983>.
 28. Cho, E. A.; Seo, J.; Lee, D. W.; Pan, J. G. Decolorization of indigo carmine by laccase displayed on *Bacillus subtilis* spores. *Enzyme Microb. Technol.* **2011**, *49*, 100–104, <https://doi.org/10.1016/j.enzmictec.2011.03.005>.
 29. Maulana, F. A. Simulasi Termostabilitas Struktur Glukosa Oksidase Aspergillus Niger IPBCC.08.610 In-Silico, IPB University, **2019**.
 30. Puspita, P. J.; Ambarsari, L.; Adiva, A.; Sumaryada, T. I. In silico analysis of glucose oxidase H516r and H516d mutations for an enzymatic fuel cell. *J. Kim. Val.* **2021**, *7*, 83–93, <https://doi.org/10.15408/jkv.v7i2.20733>.
 31. Lopes, P.; Koschorreck, K.; Nedergaard Pedersen, J.; Ferapontov, A.; Lörcher, S.; Skov Pedersen, J.; Urlacher, V. B.; Ferapontova, E. E. *Bacillus licheniformis* CotA laccase mutant: Electrocatalytic reduction of O₂ from 0.6 V (SHE) at PH 8 and in seawater. *Chem. Electro. Chem* **2019**, *6*, 2043–2049, <https://doi.org/10.1002/celec.201900363>.
 32. Koschorreck, K.; Schmid, R. D.; Urlacher, V. B. Improving the functional expression of a *Bacillus*

- licheniformis* laccase by random and site-directed mutagenesis. *BMC Biotechnol.* **2009**, *9*, <https://doi.org/10.1186/1472-6750-9-12>.
33. Pitaloka, D. A. E.; Ramadhan, D. S. F.; Arfan; Chaidir, L.; Fakhri, T. M. Docking-based virtual screening and molecular dynamics simulations of quercetin analogs as enoyl-acyl carrier protein reductase (InhA) Inhibitors of Mycobacterium Tuberculosis. *Sci. Pharm.* **2021**, *89*, <https://doi.org/10.3390/scipharm89020020>.
 34. Li, H.; Guo, L.; Ding, X.; An, Q.; Wang, L.; Hao, S.; Li, W.; Wang, T.; Gao, Z.; Zheng, Y.; Zhang, D. Molecular networking, network pharmacology, and molecular docking approaches employed to investigate the changes in *Ephedrae herba* before and after honey-processing. *Molecules* **2022**, *27*, 4057, <https://doi.org/10.3390/molecules27134057>.
 35. Ferreira De Freitas, R.; Schapira, M. A systematic analysis of atomic protein-ligand interactions in the PDB. *Medchemcomm* **2017**, *8*, 1970–1981, <https://doi.org/10.1039/c7md00381a>.
 36. Shakya, A. K. Natural phytochemicals: Potential anti-HCV Targets in silico approach. *J. Appl. Pharm. Sci.* **2019**, *9*, 94–100, <https://doi.org/10.7324/JAPS.2019.90813>.
 37. Craciun, A. M.; Rotaru, A.; Cojocar, C.; Mangalagiu, I. I.; Danac, R. New 2,9-disubstituted-1,10-phenanthroline derivatives with anticancer activity by selective targeting of telomeric g-quadruplex DNA. *Spectrochim. Acta - Part A Mol. Biomol. Spectrosc.* **2021**, *249*, 119318, <https://doi.org/10.1016/j.saa.2020.119318>.
 38. Arwansyah, A.; Ambarsari, L.; Sumaryada, T. I. Simulasi docking senyawa kurkumin dan analognya sebagai inhibitor reseptor androgen pada kanker prostat. *Curr. Biochem.* **2014**, *1*, 11–19, <https://doi.org/10.29244/cb.1.1.11-19>.
 39. Yopianto, D.; Sipangkar, M. J.; Budiyanto, R.; Siahaan, P. Studi interaksi antara segmen dimer kitosan dengan peptida Ac-CA-NH₂ dan Ac-TP-NH₂ secara komputasi Ab-Initio. *J. Kim. Sains dan Apl.* **2016**, *19*, 118–125, <https://doi.org/10.14710/jksa.19.3.118-125>.
 40. Safitri, B.; Hudiyanti, D.; Laksitorini, M. D.; Sasongko, N. A.; Siahaan, P. Intermolecular hydrogen bond interactions in n-carboxymethyl chitosan and n H₂O: DFT and NBO studies. *AIP Conf. Proc.* **2020**, 2237, <https://doi.org/10.1063/5.0005287>.
 41. Khalil, A.; El-Khouly, A. S.; Elkaeed, E. B.; Eissa, I. H. The inhibitory potential of 2'-dihalo ribonucleotides against HCV: Molecular docking, molecular simulations, mm-bpsa, and dft studies. *Molecules* **2022**, *27*, 4530, <https://doi.org/10.3390/molecules27144530>.
 42. Ahmed, S.; Ali, M. C.; Ruma, R. A.; Mahmud, S.; Paul, G. K.; Saleh, M. A.; Alshahrani, M. M.; Obaidullah, A. J.; Biswas, S. K.; Rahman, M. M.; Rahman, M. M.; Islam, M. R. Molecular docking and dynamics simulation of natural compounds from betel leaves (*Piper betle* L.) for investigating the potential inhibition of alpha-amylase and alpha-glucosidase of type 2 diabetes. *Molecules* **2022**, *27*, 4526, <https://doi.org/10.3390/molecules27144526>.
 43. Kaur, B.; Rolta, R.; Salaria, D.; Kumar, B.; Fadare, O. A.; da Costa, R. A.; Ahmad, A.; Al-Rawi, M. B. A.; Raish, M.; Rather, I. A. An in silico investigation to explore anti-cancer potential of *Foeniculum vulgare* mill. phytoconstituents for the management of human breast cancer. *Molecules* **2022**, *27*, 4077, <https://doi.org/10.3390/molecules27134077>.
 44. Bansal, R.; Mohagaonkar, S.; Sen, A.; Khanam, U.; Rathi, B. In-silico study of peptide-protein interaction of antimicrobial peptides potentially targeting SARS and SARS-CoV-2 nucleocapsid protein. *Silico Pharmacol.* **2021**, *9*, 46, <https://doi.org/10.1007/s40203-021-00103-z>.
 45. Du, J.; Qin, Y.; Wu, Y.; Zhao, W.; Zhai, W.; Qi, Y.; Wang, C.; Gao, Y. The design of high affinity human PD-1 mutants by using molecular dynamics simulations (MD). *Cell Commun. Signal.* **2018**, *16*, 1–16, <https://doi.org/10.1186/s12964-018-0239-9>.
 46. Sitthiyotha, T.; Pichyangkura, R.; Chunsriviro, S. Molecular dynamics provides insight into how N251A and N251Y mutations in the active site of *Bacillus licheniformis* RN-01 levansucrase disrupt production of long-chain levan. *PLoS One* **2018**, *13*, <https://doi.org/10.1371/journal.pone.0204915>.
 47. Shakil, S.; Danish Rizvi, S. M.; Greig, N. H. High throughput virtual screening and molecular dynamics simulation for identifying a putative inhibitor of bacterial CTX-M-15. *Antibiotics* **2021**, *10*, <https://doi.org/10.3390/antibiotics10050474>.
 48. Dehouck, Y.; Kwasigroch, J. M.; Gilis, D.; Rooman, M. PoPMuSiC 2.1: a web server for the estimation of protein stability changes upon mutation and sequence optimality. *BMC bioinformatics.* **2011**, *12*, 1-12. <https://doi.org/10.1186/1471-2105-12-151>.
 49. Song, Y.; Jiang, J.; Ma, J.; Pang, S.Y.; Liu, Y.Z.; Yang, Y.; Luo, C.W.; Zhang, J.Q.; Gu, J.; Qin, W. ABTS as an electron shuttle to enhance the oxidation kinetics of substituted phenols by aqueous permanganate. *Environmental Science & Technology.* **2015**, *49*, 11764-11771.
 50. Das, A.; Yadav, A.; Gupta, M.; Terse, V.L.; Vishvakarma, V.; Singh, S.; Nandi, T.; Banerjee, A.; Mandal, K.; Gosavi, S.; Das, R. Rational design of protein-specific folding modifiers. *Journal of the American Chemical Society.* **2021**, *143*, 18766-18776.
 51. Mousavi, S.M.; Hashemi, S.A.; Iman Moezzi, S.M.; Ravan, N.; Gholami, A.; Lai, C.W.; Chiang, W.H.; Omidifar, N.; Yousefi, K.; Behbudi, G. Recent advances in enzymes for the bioremediation of pollutants. *Biochemistry Research International.* **2021**. 1-12.

52. Strong, P.J.; Claus, H. Laccase: a review of its past and its future in bioremediation. *Critical Reviews in Environmental Science and Technology*. **2011**, *41*, 373-434.